Ferroelectric $BaTaO_2N$ Crystals Grown in a $BaCN_2$ Flux

Akira Hosono[1,], Yuji Masubuchi[2,*], Shintaro Yasui[3], Masaki Takesada[4], Takashi Endo[5], Mikio Higuchi[2], Mitsuru Itoh[3], Shinichi Kikkawa[2]*

AUTHOR ADDRESS

[1] Graduate School of Chemical Science and Engineering, Hokkaido University, N13W8, Kita-ku, Sapporo 060-8628, Japan

[2] Faculty of Engineering, Hokkaido University, N13W8, Kita-ku, Sapporo 060-8628, Japan

[3] Laboratory for Materials and Structures, Tokyo Institute of Technology, 4259, Nagatsuta-cho, Midori-ku, Yokohama 226-8503, Japan

[4] Department of Physics, Faculty of Science, Hokkaido University, N10W8, Kita-ku, Sapporo 060-0810, Japan

[5] Faculty of Engineering Technical Center, Hokkaido University, N13W8, Kita-ku, Sapporo 060-8628, Japan

ABSTRACT

Perovskite-type oxynitride $BaTaO_2N$ has been attracting attention for its large dielectric constant that is almost independent of temperature by the measurements on its ceramics. Its dielectric characteristics are attributed to polar nano regions in the average cubic crystal structure. Polarization saturation to produce butterfly-like piezoresponse force microscopy (PFM) signal was observed on $BaTaO_2N$ crystals in the present study. Reddish crystallites of $BaTaO_2N$ up to

3.1 μm in size were grown using a $BaCN_2$ flux. Grain growth proceeded through the formation of a Ruddlesden-Popper type oxynitride from the reaction between $BaTaO_2N$ powder and the molten $BaCN_2$. Their electrical property was studied using PFM with special care due to the small size of crystals. They were found to be much highly insulating than its ceramics. Ferroelectricity with a complete phase inversion was observed on oxynitride perovskite crystal for the first time. Large coercivity of 50 to 60 V was observed in the measurement. Such ferroelectricity is ascribed to the polar nano regions induced by the polar linkages between *cis*-type TaO_4N_2 octahedra.

KEYWORDS (Oxynitride, Perovskite, Metal carbodiimide, Crystal growth, Ferroelectricity).

Introduction

Metal nitrides and oxynitrides have been attracting considerable attention because they are potentially useful for their optical, electrical, magnetic and mechanical properties.[1-7] Both $SrTaO_2N$ and $BaTaO_2N$ perovskites are also important as visible light-driven photocatalysts.[8-10] They were also reported to show large relative dielectric constants with a small temperature dependence.[11] Their average crystal structures were assumed to be centrosymmetric tetragonal *I*4/*mcm* (a = 0.569411(7) nm, c = 0.80658(2) nm) for $SrTaO_2N$ and cubic *Pm*-3*m* (a = 0.41128(1) nm) for $BaTaO_2N$, based on powder neutron diffraction measurements.[12,13] Some deviations from these centrosymmetric structures have been reported that suggest local symmetry breaking, based on analyses by transmission electron microscopy (TEM) and extended X-ray absorption fine structure (EXAFS) as well as neutron pair distribution functions as crystal structural supports for the occurrence of dielectric property.[14-16] In 2011, two groups

independently reported a *cis*-type anisotropic local nitrogen configuration in TaO_4N_2 octahedra in $SrTaO_2N$ based on powder neutron diffraction studies.[17,18] These local *cis*-type units tend to align with random long-range orientation due to the similar lengths of the Ta-O and Ta-N bonds.[19,20] Relaxor-type ferroelectric behavior was expected in first-principle studies on $BaTaO_2N$ and $SrTaO_2N$ assuming the *cis*-type configuration in their TaO_4N_2 octahedra. Two types of Ta-N-Ta-N helical chain motifs switch to each other, breaking the long-range ordering of anions while retaining the local *cis*-TaO_4N_2 anisotropic configuration.[21] This disorder mechanism differs from that in typical solid solution relaxor oxide systems because the generation of compositional inhomogeneity is not necessary.[21,22]

The electrical properties of these compounds have been investigated, both as ceramics and thin films, and they have been found to be significantly affected by anion contents in the products.[6,23-28] Both $SrTaO_2N$ and $BaTaO_2N$ release a part of their nitrogen above 950 °C to change their compositions to $SrTaO_2N_{0.7}$ and $BaTaO_2N_{0.85}$, respectively, even in a nitrogen atmosphere. The green-powder compacts of these materials change from orange or reddish-coloured insulators to black semiconductors during the high temperature sintering at 1400 °C due to the partial reduction of Ta^{5+}.[23,24,27,28] The nitrogen lost from these materials can be subsequently recovered by post-ammonolysis of as-sintered ceramics at approximately 950 to 1000 °C. However, this procedure was effective only at the surface of the dense samples because it was difficult for NH_3 to reach the interiors.[23-26] Their original colors were completely recovered even in their interiors by the ammonolysis of the relatively porous ceramics. The $SrTaO_2N$ ceramic with relative density (RD) of 84.0% showed relative dielectric constants $\varepsilon_r \approx 300 – 450$ with loss $\tan\delta < 0.1$ and those of the $BaTaO_2N$ ceramic with RD of 73.0% were $\varepsilon_r \approx 290 – 620$ with $\tan\delta \approx 0.04 – 0.4$ in the temperature range from 25 – 150 °C.[23,24] These ε_r values

Table 1. Growth conditions, appearances of the products and maximum grain sizes of $BaTaO_2N$ crystals.

Product name	$BaCN_2$ amount / mol%	Duration time at 910 °C / h	Cooling rate / °C h^{-1}	Appearance after cooling	Maximum grain size / μm
As-prepared(a)	-	-	-	Reddish powder	0.2
(b)	17	0.5	1.8	Reddish powder	0.2
(c)	22	0.5	1.8	Reddish powder	0.7
(d)	36	0.5	1.8	Reddish powder	2.2
(e)	46	0.5	1.8	Reddish solid	3.1
(f)	67	0.5	1.8	Reddish solid	0.9
(g)	46	0.5	300	Reddish solid	0.5
(h)	46	24	1.8	Reddish solid	0.4

were significantly smaller than previously reported values of several thousands and the tanδ were also much smaller than the previously reported values, which well exceeded 0.1.[11] These values of the ceramics exhibited minimal changes in temperature below 150 °C.[23,24]

Piezoelectric behavior was reported on the outermost surface of dense sintered bodies of $BaTaO_2N$ and $SrTaO_2N$ with RD > 90% after their post-ammonolysis. Piezoresponse force microscopy (PFM) measurements were conducted on the thin ceramic surfaces in thickness of less than 10 μm scratched off from their bulks in the applied voltage range of ±10 V.[25,26] Clear piezoresponse images were obtained over the range of 3 to 4 V for $SrTaO_2N$ and 7 V for $BaTaO_2N$. Local hysteresis *P-E* loops were also acquired from thin specimens of a $SrTaO_2N$ ceramic using a micron-sized Pt-deposited electrode over the applied voltage range of ±12 V.[25] However, its polarization could not be saturated because a serious current leakage appeared at higher voltage than ±8 V. This is presumably because a trace amount of electrically conductive

nature is present even after post-ammonolysis of nitrogen-deficient oxynitride ceramics.[25,26] Highly-insulating and dense oxynitride samples are desired to elucidate the occurrence of polarization phase alternation by making it possible to apply high electrical voltage to the samples.

In other works, compressively strained $SrTaO_2N$ thin films also showed ferroelectric behavior[29-31] below the bias voltage range of ±8 V. It was observed only in very small domains with sizes of 10 – 100 nm and electrical leakage was observed during measurements as in the cases of the abovementioned ceramic specimens.[25,26,29] The results of density functional theory (DFT) calculations suggested that $SrTaO_2N$ film had *trans*-type anion ordering[29] and the deviation of anion distribution from *trans*- model was suggested in a $Ca_{0.5}Sr_{0.5}TaO_2N$ thin film by assuming a change of its strain.[32] The origin of the ferroelectricity in such inhomogeneous films is considered to be the compressive stress induced by the cell size mismatch between oxynitride films and oxide substrate, which cannot be determined as the intrinsic properties in oxynitride perovskites.[29-31]

The formation of self-standing single crystals with an excellent electrical insulation is necessary to investigate the intrinsic electrical properties of oxynitride perovskites. Flux growth at relatively low temperatures is a potential means of growing crystals that might otherwise thermally decompose at high temperatures. However, there is very limited information available regarding the use of fluxes to produce nitrides and oxynitrides, except for the cases of the reactions of a Na flux with several metals and oxides to grow single crystals of Ba_3ZnN_2O, Ba_4GaN_3O and Sr_4GaN_3O.[33-35] The formation of oxynitride perovskite crystals on the surfaces of single crystals of oxides such as $Sr_2Ta_2O_7$ and $La_2Ti_2O_7$ has also been reported.[1,36,37] They are considered to be grown on these oxide single crystals in alkali metal halides or molybdates

fluxes but may not be self-standing. Additionally, some effects of KCl flux on the particle morphology of $CaTaO_2N$, $SrTaO_2N$, $BaTaO_2N$, and $LaTaON_2$ were reported.[38,39] Submicron-sized cubic particles were observed, while crystals larger than several micron sizes are desirable for electrical property measurements. It should be noted that some contamination of potassium was reported in these oxynitride samples.[38] Ammonothermal method was employed to grow micron-sized oxynitride perovskite crystallites such as ABO_2N (A = Sr, Ba; B = Nb, Ta)[40], LnTaON$_2$ (Ln = La, Ce, Pr, Nd, Sm, Gd)[41], and $LaNbON_2$.[42] However, there is no reports on the electrical properties of such crystal products.

Recently, the stabilities of alkaline earth carbodiimides were investigated both experimentally and computationally to find out that tetragonal $BaCN_2$ melts at 910 °C.[43,44] Molten $BaCN_2$ was used for the crystal growth of perovskite-type $Sr_{1-x}Ba_xTaO_2N$ (x = 0.04 – 0.23) under a nitrogen flow.[44] In this work, the original $SrTaO_2N$ particles, which were round in shape and less than 100 nm in size, were partially dissolved in the $BaCN_2$ flux and crystals of the A-site substituted oxynitride perovskite $Sr_{1-x}Ba_xTaO_2N$ were grown as cubic grains with sizes up to 3.7 μm. The products had a compositional gradient from a Sr-rich interior to a Ba-rich exterior in their crystals.[44] It is therefore likely that compositionally homogeneous $BaTaO_2N$ crystals can be obtained using a similar crystal growth technique starting with $BaTaO_2N$ powder.

In the present study, small crystals of perovskite-type $BaTaO_2N$ were grown in a $BaCN_2$ flux to several micron sizes for their electrical property measurements. The crystal growth mechanism was studied by microstructural analysis of the products using transmission electron microscopy (TEM). In addition, a ferroelectric nature was clearly detected in piezoresponse force microscopic (PFM) observation on the crystals in micron size. Secondary harmonic generation (SHG) was also observed to confirm the presence of a non-centrosymmetric structure consistent

with ferroelectricity. Herein, this ferroelectric behavior is discussed on the basis of polar nano regions (PNRs) in the $BaTaO_2N$ crystal structure. This work represents the first-ever experimental demonstration to clarify the ferroelectricity of oxynitride perovskite crystals.

Experimental

Sample preparation

A reddish $BaTaO_2N$ powder was obtained using the procedure described in the **Supporting Information**. A white $BaCN_2$ powder with a tetragonal crystal structure was prepared by the ammonolysis of $BaCO_3$ powder at 900 °C for 10 h.[43,44] As-prepared $BaTaO_2N$ powder was mixed with $BaCN_2$ in 17 – 67 mol% ratio for the crystal growth in a glove box filled with a dry nitrogen, so as to avoid oxidation or hydrolysis of the $BaCN_2$. Each resulting mixture was transferred into an alumina crucible and then enclosed in a container of tantalum sheets with thicknesses of approximately 0.1 mm (Nilaco, > 99%) in a nitrogen atmosphere to suppress the loss of the $BaCN_2$ flux due to its partial vaporization or decomposition above 910 °C.[43,44]

The tantalum container was subsequently heated to 910 °C at a rate of 300 °C/h and held at that temperature for 30 min in an alumina tube furnace with a nitrogen flow of 30 mL/min. After heating, the sample was slowly cooled to 880 °C at a rate of 1.8 °C/h. In some trials, the cooling rate was increased to 300 °C/h to study the change in crystal size. The duration of the hold at 910 °C was also changed to 24 h to investigate the effect of flux loss above the melting point of $BaCN_2$, followed by cooling at a rate of 1.8 °C/h. The products were either reddish powder or solidified lumps embedding the grown crystallites, depending on the amount of $BaCN_2$ in the starting mixture. They were washed with 1 M nitric acid followed by distilled water to remove the soluble residue, consisting primarily of $BaCN_2$. A reddish powder was obtained after

filtration through filter paper with a pore size of less than 50 μm (Toyo Roshi K. K.). The preparation conditions, the product appearances after removal from the furnace, and the particle sizes of the washed final products are summarized in **Table 1**.

The crystalline phases in the products were identified using powder X-ray diffraction (XRD; Ultima IV, Rigaku) with Cu Kα radiation over the 2θ range of 10 to 90° with a step size of 0.02° and a scan rate of 10°/min. Electron probe microanalysis (EPMA; JXA-8530F, JEOL) was conducted to determine the elemental compositions of the washed crystals having grain sizes larger than 2 μm.

The average molar ratio was determined to be Ba:Ta:O:N = 23.0:22.1:37.0:17.9, which roughly corresponds to the expected stoichiometric ratio of 1:1:2:1, confirming that the product was $BaTaO_2N$. The residual carbon content was less than the detection limit (< 0.3 wt%) of CHN combustion analysis (CE440, Exeter Analytical Inc.).

Observation and Characterization

A thin slice of the $BaTaO_2N$ small crystals embedded in the solidified $BaCN_2$ (less than 100 nm thick) was prepared for TEM observations using a focused ion beam (FIB) of gallium ion (SMI 3050SE, Hitachi High-Technologies). A TEM instrument (Titan3 G2 60-300, FEI Company) equipped with a Cs-spherical aberration corrector was employed for microstructural observations of the crystals. In addition, high angle annular dark-field scanning TEM (HAADF-STEM) images were acquired using the same TEM instrument. The $BaTaO_2N$ particle sizes and their surfaces were analyzed by scanning electron microscopy (SEM; JSM-6390 LVS, JEOL). The shapes of relatively large $BaTaO_2N$ crystallites were observed with an optical microscope (VHX-2000, KEYENCE).

A spectroscopic analysis of secondary harmonic generation (SHG) by the $BaTaO_2N$ small crystals was performed to elucidate the presence of a non-centrosymmetric structure. The excitation source was an acousto-optically Q-switched Nd:YAG laser (T40-X30S-106Q, Spectra Physics) with a 1064 nm wavelength, an average power of 0.6 W and a pulse width of 30 ns at a repetition rate of 4 kHz. The laser beam was focused by a lens with a 150 mm focal length on the surface of an aggregate of $BaTaO_2N$ crystallites grown using 46 mol% $BaCN_2$ and a cooling rate of 1.8 °C/h (condition **(e)** in **Table 1**). This technique purposely used a low excitation power to avoid thermal decomposition of the $BaTaO_2N$ during irradiation and to allow data accumulation over a long time span of 4 h.

The piezoelectricity of the $BaTaO_2N$ small crystals prepared using condition **(e)** in **Table 1** was assessed using a PFM technique that is applicable to nano-sized areas in thin films avoiding some electrostatic effects to cause false detections of piezoresponse.[45-48] Prior to the present analyses, some additional processes were performed as follows; Pt was deposited by sputtering as a top electrode on the surface of $BaTaO_2N$ small crystals attached to a Cu substrate through an Au bottom electrode, to avoid any effects resulting from electrostatic forces.[46-48] Further details regarding sample processing are described in the **Supporting Information**. Switching spectroscopy piezoresponse force microscope with DART technique (SS-PFM, ASYLUM MFP-3D, Oxford Instruments) was employed in an electrical field bias of up to ±100 V through the probe coated with Ir metal (ASYELEC-01). SS-PFM was measured in a temperature range of up to 120 °C.

Results and Discussion

Characterization of the product obtained with 67 mol% $BaCN_2$

The crystalline phases of the grown product prepared using 67 mol% of $BaCN_2$ changed with its post-treatments as shown in **Figure 1**. The as-grown product was a reddish solid and its main phase was cubic $BaTaO_2N$ perovskite with a lattice parameter a = 0.4112(1) nm (**Figure 1(a)**). It was contaminated with a trace amount of the Ba-rich Ruddlesden-Popper (RP) type layered perovskite Ba_2TaO_3N along with another unidentified impurity. This Ba_2TaO_3N may have been

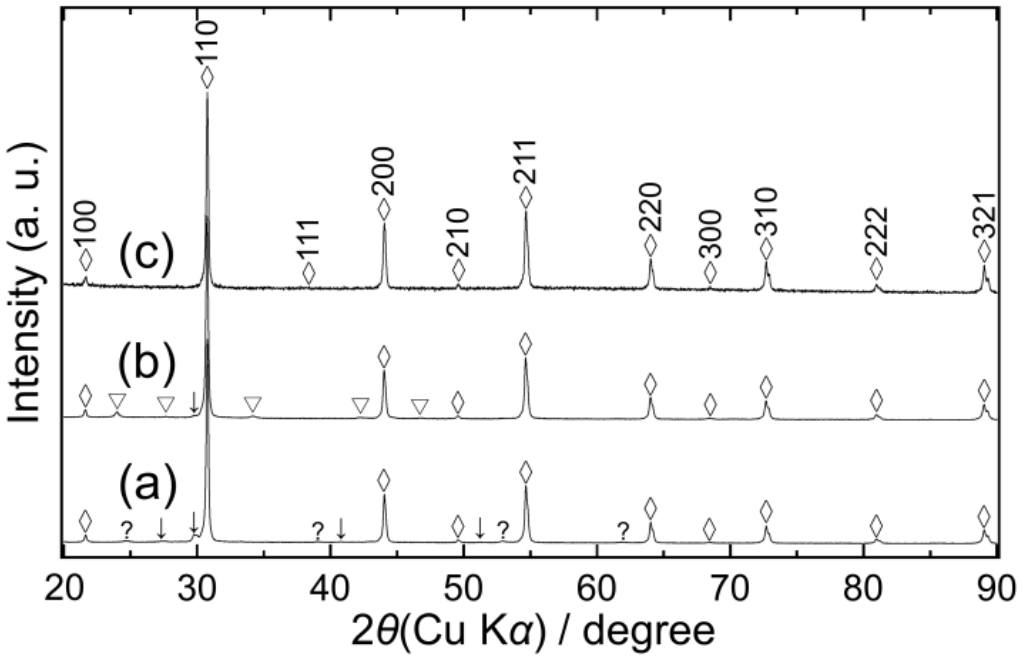

Figure 1. Powder XRD patterns of the $BaTaO_2N$ grown with 67 mol% $BaCN_2$: **(a)** as-grown product, **(b)** product after exposure to air for 1 h, and **(c)** product after washing with nitric acid and water. Diamonds, arrows, inverted triangles, and question marks indicate diffractions for $BaTaO_2N$ (ICSD 202763), Ba_2TaO_3N (JCPDS 47-1388), $BaCO_3$ (PDF 01-071-2394), and an unknown phase, respectively.

formed by the reaction of the $BaTaO_2N$ perovskite with excess Ba supplied from the $BaCN_2$ flux. Oxygen could have been incorporated from the humidity or CO_2 adsorbed at the surface of $BaTaO_2N$ and $BaCN_2$. The BaO-like intermediate reacted with $BaTaO_2N$ to form the Ba_2TaO_3N impurity, which is reported to readily decompose reacting with oxygen and humidity.[12] The Ba_2TaO_3N impurity thus almost disappeared and formed another impurity of $BaCO_3$ during the reaction in air for 1 h (**Figure 1(b)**). Diffractions of the residual $BaCN_2$ were not observed in the XRD patterns of the material likely due to the low crystallinity after the heat treatment. Finally, the crystallinity of the $BaTaO_2N$ was significantly improved after leaching of the as-grown product in nitric acid (**Figure 1(c)**). The full width at half maximum (FWHM) of the (321) diffraction peak for $BaTaO_2N$ was found to significantly decrease from 0.31° to 0.22° by the leaching process, which produced highly crystalline $BaTaO_2N$. The lattice parameter (a = 0.4111(1) nm) of the cubic $BaTaO_2N$ perovskite was determined to be consistent with the literature value (a = 0.41128 nm).[13] The cubic lattice also slightly shrank during leaching while the crystallinity was improved. These results suggest that structural defects present in the as-grown perovskite were removed by the nitric acid treatment, resulting in the formation of highly-crystalline $BaTaO_2N$. Generally, oxynitride perovskites are stable to nitric acid, but Ruddlesden-Popper phases (e. g. Sr_2TaO_3N and Ba_2TaO_3N) containing rock-salt type layers like SrO and BaO are decomposed by acid and humidity.[12,50]

The microstructure of the product prepared with 67 mol% $BaCN_2$ before nitric acid leaching was assessed. Square-shaped $BaTaO_2N$ crystals surrounded by solidified $BaCN_2$ flux are apparent in the TEM bright-field image of a thin slice of the as-grown product in **Figure 2(a)**. A selected area electron diffraction (SAED) pattern was obtained from the region indicated in this figure and the presence of cubic $BaTaO_2N$ was confirmed by applying an incident electron beam

along the <110> direction, as shown in **Figure 2(b)**. No additional diffraction spots were observed. The lattice parameter was a = 0.415(3) nm, which was in good agreement with that of the acid-washed powder sample shown in **Figure 1(c)** (a = 0.4111(1) nm) within the experimental error. A high-magnification HAADF-STEM image (**Figure 2(c)**) shows cation ordering in a portion of the encircled area in **Figure 2(a)**. Ba and Ta atoms can be distinguished in this image because their brightness levels are different as a result of the effect of their different atomic numbers on the *Z*-contrast. Specifically, the Ta atoms appear slightly brighter than the Ba atoms. The atomic arrangement in **Figure 2(c)** is consistent with a cubic perovskite-type structure observed from the <110> direction.

The crystal lattice was not well developed in the areas around the crystal edges. The area encircled in **Figure 3(a)** was observed along the <111> zone axis and the atomic arrangement in the $BaTaO_2N$ along this direction is clearly observed for the area labeled **1** at the bottom right of the higher-magnification image in **Figure 3(b)**. However, the arrangement is less clearly observed in the areas labeled **2** to **4**, which have different atomic orientations over ranges of approximately 3 to 10 nm. Fourier transformations of these images were performed using the Digital Micrograph software package (Gatan) for the areas labeled **1** to **4** in **Figure 3(b)** and the (01-1) lattice spacing was estimated from the lattice fringes indicated by the yellow arrows in this same figure. The average spacing in area **1** was determined to be 0.293 nm, which is consistent with the literature value of 0.291 nm.[13] The average spacing estimated for area **3** was slightly larger (0.316 nm). For the area **4**, the crystal orientation could not be identified from the Fourier transform image. However, the average stripe spacing in area **4** was approximately 0.333 nm, which is larger than that for area **1**. One possible explanation is that the lattice fringes in area **4** correspond to the (004) planes of RP-type Ba_2TaO_3N with space group $I4/mmm$ together with a

= 0.411508(3) nm and c = 1.33778(1) nm.[12] The c/4 value was calculated to be 0.334 nm (JCPDS 47-1388). The area out of $BaTaO_2N$ crystals therefore consists primarily of solidified $BaCN_2$ flux and $BaTaO_2N$ containing a large amount of BaO in the form of stacking defects, similar to the results obtained in work with the $SrTaO_2N$-Sr_2TaO_3N system.[50]

Ba_2TaO_3N was generated as a thin surface layer around the $BaTaO_2N$ perovskite crystals recrystallized from the $BaCN_2$ melt. In the melt, layers of Ba-rich phases such as BaO were randomly inserted between the $BaTaO_2N$ perovskite layers around the edges of the perovskite crystals. These phenomena explain why the crystallinity of the as-grown $BaTaO_2N$ was slightly low and why a trace amount of a Ba_2TaO_3N impurity is evident in the powder XRD pattern in **Figure 1(a)**. These data suggest that the starting $BaTaO_2N$ powder was dissolved to the molten $BaCN_2$ followed by the recrystallization of $BaTaO_2N$ single crystals with a uniformed perovskite-type atomic orientation and the precipitation of solid phases including Rudelesden-

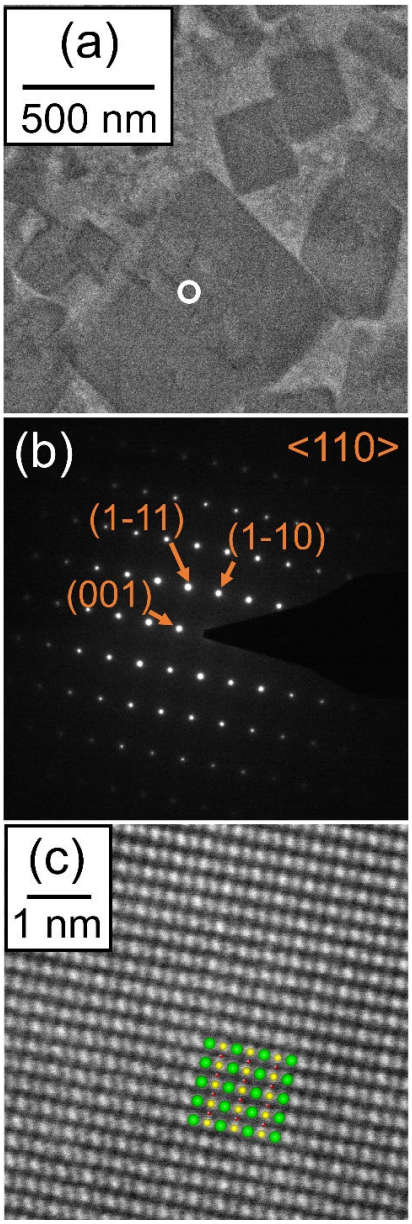

Figure 2. (a) TEM bright-field image of a thin sample specimen, **(b)** the SAED image of the area encircled in **(a)**, and **(c)** a high magnification HAADF-STEM image of the encircled area. In **(c)**, green, yellow, and red spheres indicate Ba, Ta, and O/N anions, respectively. The structural model was drawn using the VESTA software package.[49]

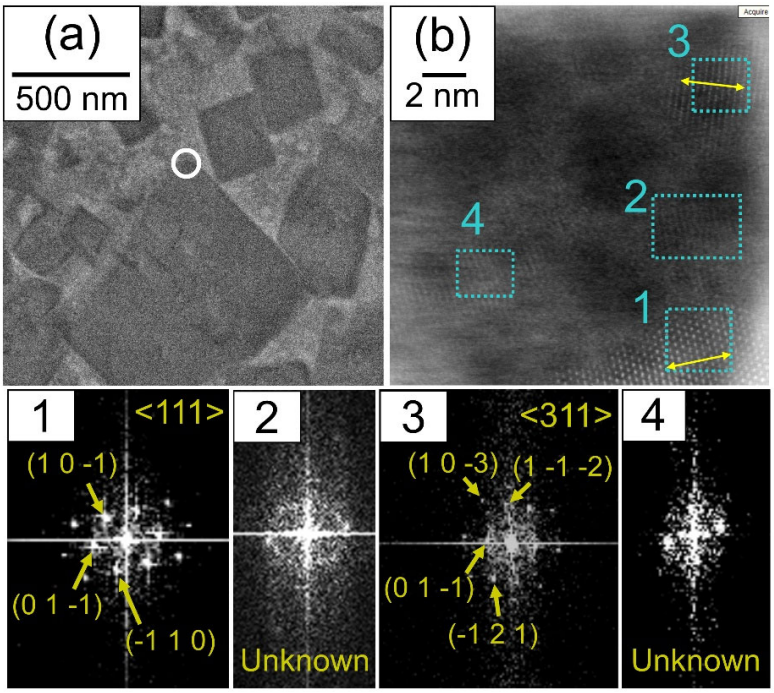

Figure 3. (a) TEM image of $BaTaO_2N$ crystals in a solidified $BaCN_2$ specimen, **(b)** HAADF-STEM image of the area encircled in **(a)**. **1** – **4** are the reciprocal Fourier transformation images generated from the regions labeled in **(b)**.

Popper type Ba_2TaO_3N which partially contain an insertion of BaO layers. The formation mechanism of Ba-rich oxynitrides such as Ba_2TaO_3N, which contains excess BaO layers between $BaTaO_2N$ can be surmised in several routes. (1) they were formed as metastable phases at the beginning of the recrystallization from the flux. These phases were generated at the interfaces between the solid $BaTaO_2N$ and the molten $BaCN_2$ during the growth of $BaTaO_2N$ crystals at high temperatures. That is, crystals of $BaTaO_2N$ did not directly recrystallize from the solution of this compound in the $BaCN_2$ flux. (2) $BaTaO_2N$ simply recrystallizes from the

$BaCN_2$ solvent and then Ba-rich phases are formed by a decomposition of $BaCN_2$ during the heating.

Growth of the $BaTaO_2N$ perovskite crystals

Some grain growth was observed in the reddish products for most of the preparation conditions in the presence of $BaCN_2$, as summarized in **Table 1**. The primary particles in the as-prepared $BaTaO_2N$ powder after ammonolysis had rounded morphologies and were 40 to 150 nm in size. These particles formed irregular aggregates approximately 2 to 3 μm in size, as depicted in **Figure 4(a)**. The shape and size of the aggregates also changed with increases in the amount of $BaCN_2$ in the flux during heating at 910 °C for 30 min. A slight crystal growth occurred in the case of the precipitation of $BaTaO_2N$ from the 17 mol% $BaCN_2$ flux (**Figure 4(b)**), while cubic crystals reflecting the euhedral form of the perovskite-type structure that appeared at 22 mol% are shown in **Figure 4(c)**. These powder products prepared with small amount of $BaCN_2$ (≤ 22 mol%) are composed of tiny particles due to a lack of flux enough to grow $BaTaO_2N$ crystallites. Larger red crystals were observed when using 46 mol% $BaCN_2$ and the particle size increased to 3.1 μm at 46 mol% $BaCN_2$, as can be seen in **Figure 4(e)**. Micron-sized $BaTaO_2N$ crystals were grown only in the cases which the exterior region of the original $BaTaO_2N$ particles were dissolved to the $BaCN_2$ flux and interior of the $BaTaO_2N$ particles are remained as the nucleus for the crystal growth. In the samples containing micron-sized $BaTaO_2N$ crystals (**Fig. 4(d)** and **(e)**), large crystals several microns in size coexisting with many submicron particles were observed. Slow precipitation from a dilute $BaTaO_2N$ solution in the $BaCN_2$ flux was expected to increase the crystal size. Rather, aggregates of small cubic crystals were present when using high $BaCN_2$ concentrations (≥ 67 mol%), as depicted in **Figure 4(f)**.

The original $BaTaO_2N$ powder was completely dissolved in a large amount of molten $BaCN_2$ at high temperatures and tiny particles recrystallized by homogeneous nucleation.

In one trial, the cooling rate was increased from 1.8 to 300 °C/h using 46 mol% $BaCN_2$. Under these conditions, the crystal size was found to decrease to less than 0.5 μm, as shown in **Figure 4(g)**. This suggests that slow cooling is required to obtain larger $BaTaO_2N$ crystals from a $BaCN_2$ flux. The effect of the hold duration at 910 °C was also investigated by changing the hold time from 30 min to 24 h using the 46 mol% $BaCN_2$. The maximum particle size from this trial was only 0.4 μm, as is evident in **Figure 4(h)**. The formation of much smaller crystals as compared to those obtained after 30 min (**Figure 4(e)**) is attributed to a partial loss of the molten $BaCN_2$ flux by evaporation and decomposition during the heating process.[43,44] Heating the reaction system to the melting point of tetragonal $BaCN_2$ (910 °C)[43,44] is necessary to dissolve $BaTaO_2N$ powder, but the duration at 910 °C should be as short as possible because $BaCN_2$ flux is lost above 910 °C, which results in a condensation of the solution to form only tiny crystallites. Therefore, it is important to maintain a sufficient amount of the $BaCN_2$ melt during the crystal growth, even though this is difficult in practice.

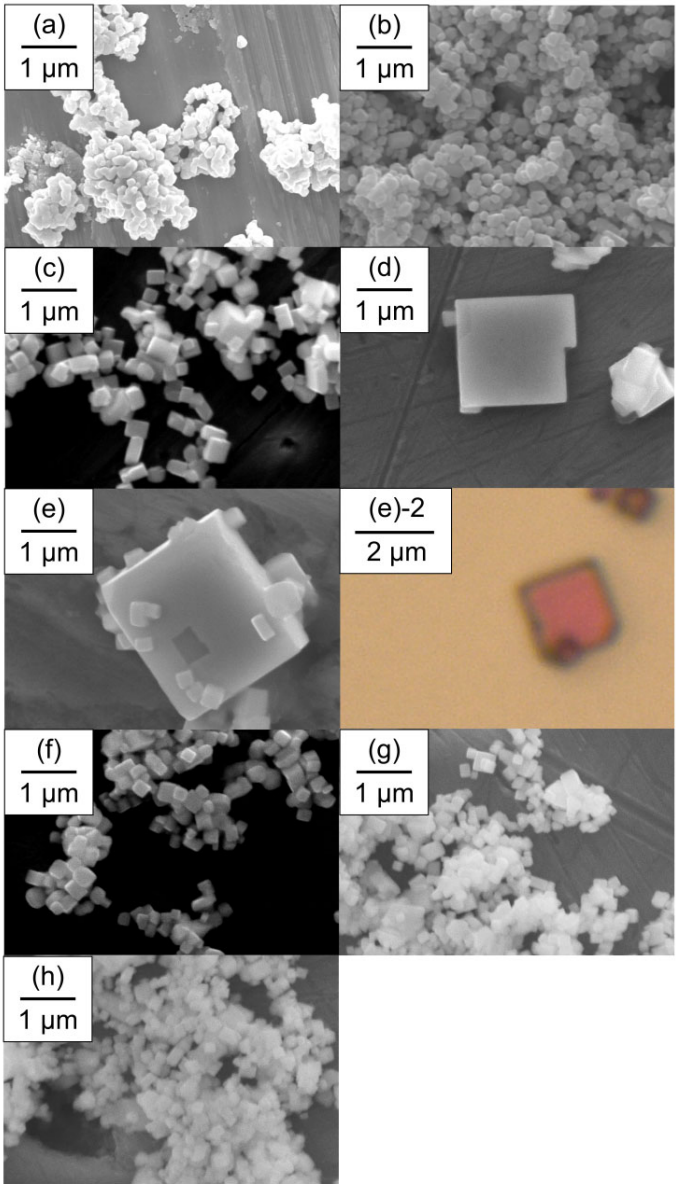

Figure 4. SEM micrographs of $BaTaO_2N$ particles. **(a)** The as-prepared ammonolysis product, **(b)** – **(f)** the products generated in flux at 910 °C for 30 min with 17, 22, 36, 46, and 67 mol% $BaCN_2$, respectively, after cooling at 1.8 °C/h and acid/water washing, and similar products obtained using 46 mol% $BaCN_2$ at 910 °C **(g)** for 30 min with cooling at 300 °C/h and **(h)** for 24 h with the rate of 1.8 °C/h. **(e)-2** an optical micrograph of the product **(e)**.

Piezoelectric analyses of $BaTaO_2N$ single crystals

Reddish $BaTaO_2N$ crystals grown with 46 mol% $BaCN_2$, a 30 min hold at 910 °C and a cooling rate of 1.8 °C/h, which were several microns in size, were assessed by applying PFM because they were not large enough for an ordinary measurement of electrical property. After leaching with nitric acid, these crystals were found to consist of phase-pure $BaTaO_2N$ perovskite (see **Figure S2** in the **Supporting Information**) with lattice parameter a = 0.41118(3) nm, which is consistent with the literature value (a = 0.41128 nm).[13] The crystals were cubic, reflecting the cubic lattice in the average structure, although local symmetry breaking in the *cis*-type configuration around TaO_4N_2 octahedra has been reported. Prior to studying piezoelectric properties, SHG assessments were performed for $BaTaO_2N$ crystals obtained under the same conditions to confirm the presence of non-centrosymmetric structure for ferroelectricity. In these trials, a 1064 nm laser beam with a diameter of approximately 100 μm was irradiated to the surface of the $BaTaO_2N$ crystal aggregate at 30 °C, to avoid the partial loss of nitrogen from the crystals as a result of laser heating. In response, a weak secondary harmonic wave at 532 nm was observed (**Figure 5(a)**), confirming the presence of non-centrosymmetric regions in the $BaTaO_2N$ crystals. This result demonstrates that local symmetry was disturbed by the co-presence of oxygen and nitrogen atoms in the reported centrosymmetric *Pm*-3*m* crystal structure. This nonlinear optical effect is consistent with the occurrence of the ferroelectric piezoresponse discussed below.

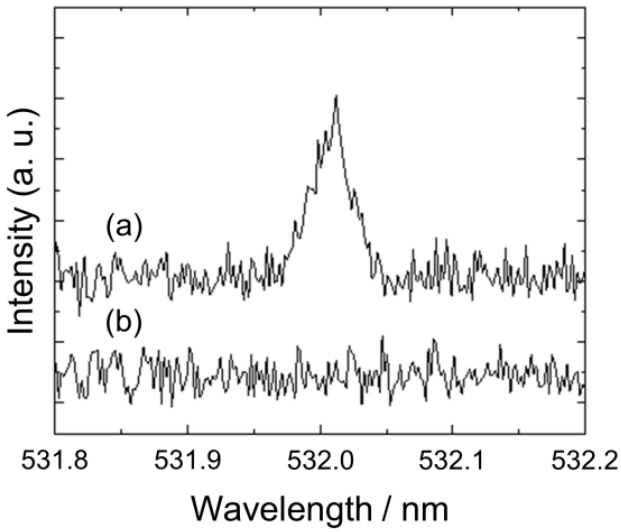

Figure 5. SHG spectra acquired from **(a)** $BaTaO_2N$ crystal aggregates and **(b)** reference amorphous silicon dioxide powder at room temperature.

Electrical short was avoided by forming island structure, which is fabricated by the FIB grooving of connected Pt deposited side-wall to bottom Au electrode and copper substrate (see **Figure S1**). A square region with dimensions of 2.5 x 2.0 μm^2 was found out in the AFM topographical image of a $BaTaO_2N$ single crystal and covered with a Pt top electrode, as shown in **Figure 6(a)**. An AC electrical voltage of 2Vp-p (peak to peak voltage) was subsequently applied to the present crystal at various temperatures. It was found that a much higher electrical voltage could be applied to the present highly-insulating crystals than the previous ceramic samples, which showed serious current leakage at voltages as low as 10 V.[25,26] Hysteresis loops were observed in the piezoresponse over the temperature range of 30 to 90 °C under electrical voltage of less than 40 V, but there was no polarization switching over the voltage range applied. PFM phase hysteresis loop and PFM amplitude butterfly curve originated from ferroelectricity

were clearly observed at 120 °C in an applied electrical voltage of ±100 V as shown in **Figure 6(b)** and **6(c)**. The maximum applied electric field was roughly estimated as 460 kV/cm. The coercive voltage was 50 to 60 V according to the phase and amplitude signals, although a higher voltage was required to induce clear piezoresponse phase switching.

Note that electrostrictive effect was observed in amplitude curve due to an application of very high voltage. Here, polarization(*P*)-electric field(*E*) hysteresis loop should be measured, however it is very difficult to execute due to following reasons; (1) enough charge could not be obtained using island system because of very small top electrode size, and (2) artificial charge from air capacitor between cantilever and top electrode might be included in measurement. Reliable capacitance value could not be obtained due to the same reason with (1). Therefore, although we could not measure exact *P-E* hysteresis loop, clear polarization switching was obtained in this SS-PFM measurement, indicating that $BaTaO_2N$ crystal is truly ferroelectric material.

The observed ferroelectric polar phase alternation is consistent with the presence of PNRs in the $BaTaO_2N$, which has previously been suggested by many researchers as indicating the favorability of *cis*-type anisotropic anion configurations and the formation of spontaneous polarization in oxynitride perovskites (**Figure 7(a)**).[17,18,21] Previous neutron diffraction analyses have found that the average crystal structure of

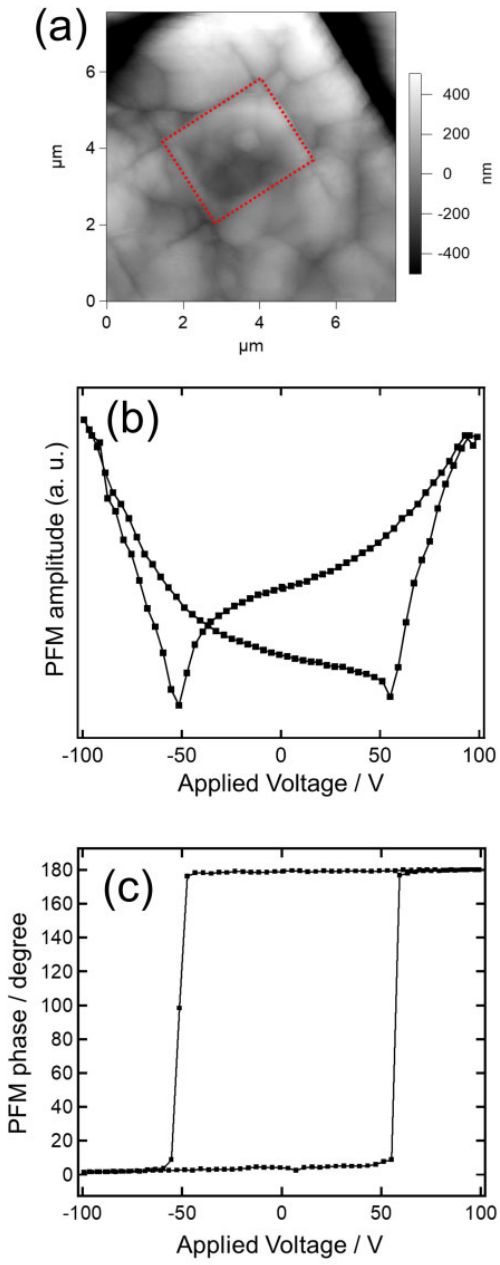

Figure 6. (a) AFM topographical image of a $BaTaO_2N$ crystal (indicated by the dotted red square), **(b)** piezoresponse amplitude curve obtained at 120 °C, and **(c)** its ferroelectric phase signal graph.

$BaTaO_2N$ is that of a cubic perovskite with space group *Pm*-3*m* and a = 0.41128 nm[13], in which nitrogen atoms are randomly present, together with oxygen atoms, at 3*c* sites. However, this compound has also been assumed to contain TaO_4N_2 octahedra having *cis*-type coordination, similar to tetragonal $SrTaO_2N$.[21] The nitrogen atoms form the *cis*-type configurations to consist the helical Ta-N chain motifs in the apical linkages to TaO_4N_2 octahedra. The PNRs in **Figure 7(a)** are formed by the interaction between two kinds of helical Ta-N chain coil motifs; clockwise and anti-clockwise. These are present in the domain structures of PNRs even at room temperature, which is below the Burn's temperature for this compound (**Figure 7(b)**).[51] The concentration of these PNRs is low, as suggested by the weak intensity of the SHG signal shown in **Figure 5(a)**, because the domains are almost averaged in the total crystal structure. The polar domain size gradually grows with increases in the applied electrical field bias, as summarized schematically in **Figure 7(c)** and **7(d)**.

In a preliminary experiment, polarization phase alternation was observed at high temperature (e. g. 100 °C), while no phase switching was detected in the same voltage range at 30 °C. This suggests that polarization phase in PNRs could be more easily altered by the assist of heat as in the case of typical relaxor ferroelectrics like $Pb(Mg_{1/3}Nb_{2/3})O_3$.[52] The polarization was saturated above ±60 V in the applied electric field to show the clear ferroelectric piezoresponse at approximately 100 °C. The present crystals were sufficiently insulating so as to allow the application of electrical fields as high as ±100 V, which is by far higher than the maximum values previously reported for ceramic samples (up to approximately ±10 V).[25,26] This characteristic enabled saturation of the polarization of $BaTaO_2N$ crystals to produce

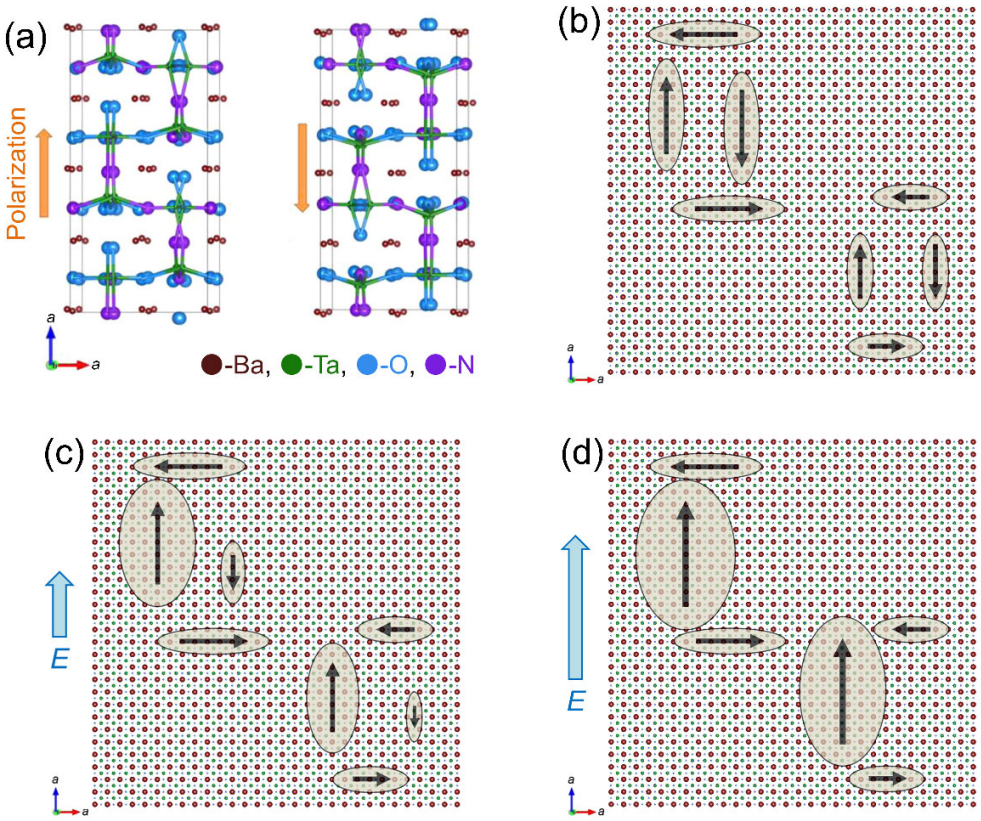

Figure 7. (a) Two sets of polar nano regions in the crystal structure of $BaTaO_2N$ with *cis*-type anion ordering as simulated by molecular dynamics calculations. Brown, green, blue, and purple spheres indicate Ba, Ta, O, and N, respectively. A part of **(a)** is reproduced from ref. 21 with the permission of the American Chemical Society. Structural models were drawn using the VESTA software package[49], **(b)** polar nano regions present in the average *Pm*-3*m* cubic crystal lattice in which most of the oxygen and nitrogen atoms are randomly distributed at 3*c* sites, **(c)** polar nano regions growing along the applied electric field, and **(d)** the polarization saturated at applied electric fields higher than ±60 V.

clear butterfly-like PFM signals. Investigations of the structures of $BaTaO_2N$ single crystals after the polarization process are now under investigation.

Conclusions

Small cubic crystals of perovskite-type $BaTaO_2N$ were grown to a size of approximately 3.1 μm in molten $BaCN_2$. The crystal growth is considered to proceed through the formation of Ba-rich Ba_2TaO_3N. Maintaining the $BaCN_2$ melt for a prolonged time span was an effective means of promoting crystal growth. These small $BaTaO_2N$ crystals showed a clear ferroelectric piezoresponse, indicating the presence of polarization that could be switched by applying an external electrical field at 120 °C in PFM measurement. This polarization switching of self-standing oxynitride perovskite without electrical leakage was observed for the first time. This finding clearly confirmed the ferroelectric properties of this material in conjunction with polar nano regions. The co-presence of nitrogen with oxygen in the centrosymmetric average crystal structure of oxynitride perovskites partially lowered the local crystal symmetry to produce polar nano regions with a non-centrosymmetric structure. These results should assist in identifying a number of new ferroelectric materials based on mixed anion compounds especially oxynitrides.

ASSOCIATED CONTENT

Supporting Information

Following files are available free of charge.

1. Synthetic procedure of $BaTaO_2N$ powder.

2. Electrode preparation process on $BaTaO_2N$ crystal surface.

3. Powder XRD profile of $BaTaO_2N$ crystals.

All the contents are included in one PDF file.

AUTHOR INFORMATION

Corresponding Authors

*Akira Hosono; E-mail: ezohakitaguni@frontier.hokudai.ac.jp

*Yuji Masubuchi; E-mail: yuji-mas@eng.hokudai.ac.jp

Author Contributions

This research was mainly conducted by A.H., Y.M. and S.K. All of authors contributed to paper preparation. The growth of $BaTaO_2N$ crystals and XRD analyses were conducted by A.H. SHG measurements were performed under supervision of M.T. Elemental analyses of $BaTaO_2N$ crystals and mono-layered capacitor fabrication was performed with the by technical assistance of T.E. PFM measurements were performed by A.H., S.Y., and M.I.

Funding Sources

This research was supported in part by a KAKENHI Grant-in-Aid for Scientific Research (A) (no. 24245039), a Research Fellowship (no. 19J10301), and a grant for Scientific Research on Innovative Areas “Mixed Anion” (no. JP16H06439) from the Japan Society for the Promotion of Science (JSPS), and as a part of the “Nanotechnology Platform” Program of the Ministry of Education, Culture, Sports, Science and Technology (MEXT), Japan (grant no. A-18-HK-00100), and Collaborative Research Project of Laboratory for Materials and Structures, Tokyo Institute of Technology.

ACKNOWLEDGMENT

SHG measurements were technically supported by Hiroki Mizuno and Kazuki Shimizu (Division of Physics, Faculty of Science, Hokkaido University). The TEM observations were conducted with the assistance of Ryo Ohta (Hokkaido University Faculty of Engineering Technical Center, Japan).

ABBREVIATIONS

TEM, transmission electron microscope; EXAFS, extended X-ray absorption fine structure; RD, relative density; PFM, piezoresponse force microscopy; SHG; secondary harmonic generation; PNRs, polar nano regions.

REFERENCES

[1] S. G. Ebbinghaus, H. -P. Abicht, R. Dronskowski, T. Muller, A. Reller, A. Weidenkaff, "Perovskite-related oxynitrides - recent developments in synthesis, characterization and investigations of physical properties", *Prog. Solid State Chem.*, 2009, 37, 173–205.

[2] M. Jansen, H. P. Letschert, "Inorganic yellow-red pigments without toxic metals", *Nature*, 2000, 404, 980–982.

[3] R. Aguiar, D. Logvinovich, A. Weidenkaff, A. Rachel, A. Reller, S. G. Ebbinghaus, "The vast colour spectrum of ternary metal oxyniride pigments", *Dyes Pigment.*, 2008, 76, 70–75.

[4] T. Takeda, R. Xie, T. Suehiro, N. Hirosaki, "Nitride and oxynitride phosphors for white LEDs: Synthesis, new phosphor discovery, crystal structure", *Prog. Solid State Chem.*, 2018, 51, 41–51.

[5] M. Zeuner, S. Pagano, W. Schnick, "Nitridosilicates and Oxonitridosilicates: From Ceramic Materials to Structural and Functional Diversity", *Angew. Chem. Int. Ed.*, 2011, 50, 7754–7775.

[6] S. Kikkawa, A. Hosono, Y. Masubuchi, "Remarkable effects of local structure in tantalum and niobium oxynitrides", *Prog. Solid State Chem.*, 2018, 51, 71–80.

[7] S. Kikkawa, Y. Masubuchi, *Prog. Solid State Chem.*, "Magnetic iron nitrides inspired by historic research on α''-$Fe_{16}N_2$", 2018, 51, 19–26.

[8] K. Maeda, K. Domen, "Water Oxidation Using a Particulate $BaZrO_3$-$BaTaO_2N$ Solid-Solution Photocatalyst That Operates under a Wide Range of Visible Light", *Angew. Chem. Int. Ed.*, 2012, 51, 9865–9869.

[9] M. Higashi, R. Abe, K. Teramura, T. Takata, B. Ohtani, K. Domen, "Two step water splitting into H_2 and O_2 under visible light by $ATaO_2N$ (A = Ca, Sr, Ba) and WO_3 with IO_3^-/I^- shuttle redox mediator", *Chem. Phys. Lett.*, 2008, 452, 120–123.

[10] K. Ueda, T. Minegishi, J. Clune, M. Nakabayashi, T. Hisatomi, H. Nishiyama, M. Katayama, N. Shibata, J. Kubota, T. Yamada, K. Domen, "Photoelectrochemical Oxidation of Water Using $BaTaO_2N$ Photoanodes Prepared by Particle Transfer Method", *J. Am. Chem. Soc.*, 2015, 137, 2227–2230.

[11] Y. -I. Kim, P. M. Woodward, K. Z. Baba-Kishi, C. W. Tai, "Characterization of the Structural, Optical, and Dielectric Properties of Oxynitride Perovskites AMO_2N (*A* = Ba, Sr, Ca; *M* = Ta, Nb)", *Chem. Mater.*, 2004, 16**,** 1267–1276.

[12] S. J. Clarke, K. A. Hardstone, C. W. Michie, M. J. Rosseinski, "High-temperature synthesis and structures of perovskite and n=1 Ruddlesden-Popper tantalum oxynitrides", *Chem. Mater.*, 2002, 14, 2664–2669.

[13] F. Pors, R. Marchand, Y. Laurent, "Structural study of $BaTaO_2N$ and $BaNbO_2N$ oxynitrided perovskites", *Mat. Res. Bull.*, 1988, 23, 1447–1450.

[14] K. Page, M. Stoltzfus, Y. -I, Kim, T. Proffen, P. M. Woodward, A. K. Cheetham, R. Seshadri, "Local atomic ordering in $BaTaO_2N$ studied by neutron pair distribution function analysis and density function theory", *Chem. Mater.*, 2007, 19, 4037–4042.

[15] R. L. Withers, Y. Liu, P. M. Woodward, Y. I. Kim, "Structurally frustrated polar nanoregions in $BaTaO_2N$ and the relationship between its high dielectric permittivity and that of $BaTiO_3$", *App. Phys. Lett.*, 2008, 92, 102907.

[16] B. Ravel, Y. I. Kim, P. M. Woodward, C. M. Fang, "Role of local disorder in the dielectric response of $BaTaO_2N$", *Phys. Rev. B*, 2006, 73, 184121.

[17] M. Yang, J. Oro-Sole, J. A. Rodgers, A. Jorge, A. Fuertes, J. P. Attfield, "Anion order in perovskite oxynitrides", *Nat. Chem.*, 2011, 3, 47–52.

[18] Y. -R. Zhang, T. Motohashi, Y. Masubuchi and S. Kikkawa, "Local anionic ordering and anisotropic displacement in dielectric perovskite $SrTaO_2N$", *J. Cer. Soc. Jpn.*, 2011, 119, 581–586.

[19] J. P. Attfield, "Principles and Applications of Anion Order in Solid Oxynitrides", *Cryst. Growth Des.*, 2013, 13, 4623–4629.

[20] C. M. Fang, G. A. Wijs, E. Orhan, G. With, R. A. Groot, H. T. Hintzen, R. Marchand, "Local Structure and electronic properties of $BaTaO_2N$ with perovskite-type structure", *J. Phys. Chem. Solid*, 2003, 64, 281–286.

[21] Y. Hinuma, H. Moriwake, Y. Zhang, T. Motohashi, S. Kikkawa, I. Tanaka, "First principles study on relaxor-type ferroelectric behavior without chemical inhomogeneity in $BaTaO_2N$ and $SrTaO_2N$", *Chem. Mater.*, 2012, 24, 4343–4349.

[22] A. A. Bokov, Z. –G. Ye, “Recent progress in relaxor ferroelectrics with perovskite structure”, *J. Mater. Sci.*, 2006, 41, 31–52.

[23] S. -K. Sun, Y. -R. Zhang, Y. Masubuchi, T. Motohashi, S. Kikkawa, “Additive sintering, postannealing, and dielectric properties of $SrTaO_2N$”, *J. Am. Ceram. Soc.*, 2014, 97, 1023–1027.

[24] A. Hosono, S. -K. Sun, Y. Masubuchi, S. Kikkawa, “Additive sintering and post-ammonolysis of dielectric $BaTaO_2N$ oxynitride perovskite”, *J. Eur. Ceram. Soc.*, 2016, 36, 3341–3345.

[25] S. Kikkawa, S. -K. Sun, Y. Masubuchi, Y. Nagamine, T. Shibahara, “Ferroelectric response induced by *cis*-type anion ordering in $SrTaO_2N$ oxynitride perovskite”, *Chem. Mater.*, 2016, 28, 1312–1317.

[26] A. Hosono, Y. Masubuchi, Y. Nagamine, T. Shibahara, S. Kikkawa, “Piezoresponse and microstructure of $BaTaO_2N$ ceramics”, *J. Eur. Ceram. Soc.*, 2018, 38, 3478–3482.

[27] Y. -R. Zhang, T. Motohashi, Y. Masubuchi, S. Kikkawa, “Sintering and Dielectric Properties of Perovskite $SrTaO_2N$ Ceramics” *J. Eur. Ceram. Soc.*, 2012, 32, 1269–1274.

[28] D. Chen, D. Habu, Y. Masusbuchi, S. Torii, T. Kamiyama, S. Kikkawa, “Partial nitrogen loss in $SrTaO_2N$ and $LaTiO_2N$ oxynitride perovskites”, *Solid State Sci.*, 2016, 54, 2–6.

[29] D. Oka, Y. Hirose, T. Fukumura, K. Sasa, S. Ishii, H. Matsuzaki, Y. Sato, Y. Ikuhara, T. Hasegawa, “Possible ferroelectricity in perovskite oxynitride $SrTaO_2N$ epitaxial thin films”, *Sci. Rep.*, 2014, 4, 4987.

[30] C. L. Paven, R. Benzerga, A. Ferri, D. Fasquelle, V. Laur, L. L. Gendre, F. Marlec, F. Tessier, F. Cheviré, R. Desfeux, S. Saitzek, X. Castel, A. Sharaiha, “Ferroelectric and dielectric study of strontium tantalum based perovskite oxynitride films deposited by reactive rf magnetron sputtering”, *Mat. Res. Bull.*, 2017, 96, 126–132.

[31] F. Marlec, C. L. Paven, L. L. Gendre, R. Benzerga, F. Cheviré, F. Tessier, F. Gam, A. Sharaiha, “Deposition and dielectric study as function of thickness of perovskite oxynitride $SrTaO_2N$ thin films elaborated by reactive sputtering”, *Surf. Coat. Technol.*, 2017, 324, 607–613.

[32] D. Oka, Y. Hirose, F. Matsui, H. Kamisaka, T. Oguchi, N. Maejima, H. Nishikawa, T. Muro, K. Hayashi, T. Hasegawa, Strain Engineering for Anion Arrangement in Perovskite Oxynitrides, *ACS Nano*, 2017, 11, 3860–3866.

[33] H. Yamane, F. J. DiSalvo, “Synthesis and crystal structure of new oxynitride, Ba_3ZnN_2O”, *J. Alloys Compd.*, 1996, 234, 203–206.

[34] T. Hashimoto and H. Yamane, “Ba_4GaN_3O”, *Acta Cryst.*, 2014, E70, i28.

[35] P. M. Mallinson, Z. A. Gàl, S. J. Clarke, “Two New Structurally Related Strontium Gallium Nitrides: Sr_4GaN_3O and $Sr_4GaN_3(CN_2)$”, *Inorg. Chem.*, 2006, 45, 419–423.

[36] M. Hojamberdiev, A. Yamaguchi, K. Yubuta, S. Oishi, K. Teshima, “Fabrication of $La_2Ti_2O_7$ Crystals Using an Alkali-Metal Molibdate Flux Growth Method and Their Nitridability To Form

$LaTiO_2N$ Crystals under a High-Temperature NH_3 Atmosphere", *Inorg. Chem.*, 2015, 54, 3237–3244.

[37] Y. Mizuno, H. Wagata, K. Yubuta, N. Zettsu, S. Oishi, K. Teshima, "Flux Growth of $Sr_2Ta_2O_7$ crystals and subsequent nitridation to form $SrTaO_2N$ crystals", *CrystEngComm*, 2013, 15, 8133–8138.

[38] M. Hojamberdiev, K. Yubuta, J. M. Vequizo, A. Yamakata, S. Oishi, K. Domen, K. Teshima, "NH_3-Assisted Flux Growth of Cube-like $BaTaO_2N$ Submicron Crystals in a Completely Ionized Nonaqueous High-Temperature Solution and Their Water Splitting Activity", *Cryst. Growth Des.*, 2015, 15, 4663–4671.

[39] Y. -I. Kim, "Effects of KCl flux on the morphology, anion composition, and chromaticity of perovskite oxynitrides, $CaTaO_2N$, $SrTaO_2N$, and $LaTaON_2$", *Ceram. Int.*, 2014, 40, 5275–5281.

[40] N. Cordes, T. Bräuniger, W. Schnick, "Ammonothermal Synthesis of $EAMO_2N$ (*EA* = Sr, Ba; *M* = Nb, Ta) Perovskites and ^{14}N Solid-State NMR Spectroscopic Investigations of $AM(O,N)_3$ (*A* = Ca, Sr, Ba, La)", *Eur. J. Inorg. Chem.*, 2018, 5019–5026.

[41] N. Cordes, W. Schnick, "Ammonothermal Synthesis of Crystalline Oxonitride Perovskites $LnTaON_2$ (Ln = La, Ce, Pr, Nd, Sm, Gd)", *Chem. Eur. J.*, 2017, 23, 11410–11415.

[42] C. Izawa, T. Kobayashi, K. Kishida, T. Watanabe, "Ammonothermal Synthesis and Photocatalytic Activity of Lower Valence Cation-Doped $LaNbON_2$", *Adv. Mat. Sci. Engin.*, 2014, 465720.

[43] A. Hosono, R. P. Stoffel, Y. Masubuchi, R. Dronskowski, S. Kikkawa, "Melting Behavior of Alkaline-Earth Metal Carbodiimides and Their Thermochemisty from First-Principles", *Inorg. Chem.*, 2019, 58, 8938–8942.

[44] A. Hosono, Y. Masubuchi, T. Endo, S. Kikkawa, "Molten $BaCN_2$ for the sintering and crystal growth of dielectric oxynitride perovskite $Sr_{1-x}Ba_xTaO_2N$ (x = 0.04~0.23)", *Dalton Trans.*, 2017, 46, 16837–16844.

[45] D. A. Bonnell, S. V. Kalinin, A. L. Kholkin, A. Gruverman, "Piezoresponse Force Microscopy: A Window into Electromechanical Behavior at the Nanoscale", *MRS Bulletin*, 2009, 34, 648–657.

[46] D. Seol, B. Kim, Y. Kim, "Non-piezoelectric effects in piezoresonse force microscopy", *Curr. Appl. Phys.*, 2017, 17, 661–674.

[47] N. Faraji, Z. Yan, J. Seidel, "Electrical conduction at domain walls in lead titanate ($PbTiO_3$) single crystals", *Appl. Phys. Lett.*, 2017, 110, 213108.

[48] J. Seidel, L. W. Martin, Q. He, Q. Zhan, Y. -H. Chu, A. Rother, M. E. Hawkridge, P. Maksymovych, P. Yu, M. Gajek, N. Balke, S. V. Kalinin, S. Gemming, F. Wang, G. Catalan, J. F. Scott, N. A. Spaldin, J. Orestein, R. Ramesh, "Conduction at domain walls in oxide multiferroics", *Nat. Mater.*, 2009, 8, 229–234.

[49] K. Momma, F. Izumi, "VESTA 3 for three-dimensional visualization of crystal, volumetric and morphology data", *J. Appl. Crystallogr.*, 2011, 44, 1272–1276.

[50] Y. Suemoto, Y. Masubuchi, Y. Nagamine, A. Matsutani, T. Shibahara, K. Yamazaki, S. Kikkawa, "Intergrowth between the Oxynitride Perovskite $SrTaO_2N$ and the Ruddlesden-Popper Phase Sr_2TaO_3N", *Inorg. Chem.*, 2018, 57, 9086–9095.

[51] G. Burns, F. H. Dacol, "Crystalline ferroelectrics with glassy polarization behavior", *Phys. Rev. B*, 1983, 28, 2527–2530.

[52] D. Fu, H. Taniguchi, M. Itoh, S. Koshihara, N. Yamamoto, S. Mori, "Relaxor $Pb(Mg_{1/3}Nb_{2/3})O_3$: A Ferroelectric with Multiple Inhomogeneities", *Phys. Rev. Lett.*, 2009, 103, 207601.

SYNOPSIS

Reddish cubic crystallites of perovskite-type $BaTaO_2N$ were grown up to 3.1 μm in size using $BaCN_2$ as a flux. Ferroelectric piezoresponse with a clear polarization phase switching was observed on the oxynitride crystals for the first time in PFM. The ferroelectricity is consistent with the previously suggested local symmetry breaking due to the anisotropic anion ordering in centrosymmetric average structure.